Journal of Alloys and Compounds 509 (2011) 8158–8164

Contents lists available at ScienceDirect

Journal of Alloys and Compounds

journal homepage: www.elsevier.com/locate/jallcom

Photocatalytic performance of nano-photocatalyst from TiO_2 and Fe_2O_3 by mechanochemical synthesis

Tanmay K. Ghorai[a,b,*], Mukut Chakraborty[a], Panchanan Pramanik[b]

[a] Department of Chemistry, West Bengal State University, Barasat, North 24 Pgs, Kolkata 700126, India
[b] Department of Chemistry, Indian Institute of Technology Kharagpur, Kharagpur 721302, India

ARTICLE INFO

Article history:
Received 7 September 2010
Received in revised form 14 May 2011
Accepted 17 May 2011
Available online 1 June 2011

Keywords:
Solid solution
Fe_2O_3/TiO_2
Nanocatalysts
Photooxidation

ABSTRACT

Nano-particles of homogeneous solid solution between TiO_2 and Fe_2O_3 (up to 10 mol%) have been prepared by mechanochemical milling of TiO_2 and yellow Fe_2O_3/red Fe_2O_3/precipitated Fe $(OH)_3$ using a planetary ball mill. Such novel solid solution cannot be prepared by conventional co-precipitation technique. A preliminary investigation of photocatalytic activity of mixed oxide (TiO_2/Fe_2O_3) on photo-oxidation of different organic dyes like Rhodamine B (RB), Methyl orange (MO), Thymol blue (TB) and Bromocresol green (BG) under visible light (300-W Xe lamp; $\lambda > 420$ nm) showed that TiO_2 having 5 mol% of Fe_2O_3 (YFT1) is 3–5 times higher photoactive than that of P25 TiO_2. The XRD result did not show the peaks assigned to the Fe components (for example Fe_2O_3, Fe_3O_4, FeO_3, and Fe metal) on the external surface of the anatase structure in the Fe_2O_3/TiO_2 attained through mechanochemical treatment. This meant that Fe components were well incorporated into the TiO_2 anatase structure. The average crystallite size and particle size of YFT1 were found to be 12 nm and 30 ± 5 nm respectively measured from XRD and TEM conforming to nanodimensions. Together with the Fe component, they absorbed wavelength of above 387 nm. The band slightly shifted to the right without tail broadness, which was the UV absorption of Fe oxide in the Fe_2O_3/TiO_2 particle attained through mechanochemical method. This meant that Fe components were well inserted into the framework of the TiO_2 anatase structure. EPR and magnetic susceptibility show that Fe^{3+} is in low spin state corresponding to $\mu_B = 1.8$ BM. The temperature variation of μ_B shows that Fe^{3+} is well separated from each other and does not have any antiferromagnetic or ferromagnetic interaction. The evidence of Fe^{3+} in TiO_2/Fe_2O_3 alloy is also proved by a new method that is redox titration which is again support by the XPS spectrum.

1. Introduction

Photocatalytic oxidation of organic compound by wide band gap semiconductor studies is an important area of investigation. In this regard studies with TiO_2 and modified TiO_2 are area of intense investigation [1–10].

The photocatalytic property of a multicomponent system is strongly influenced by the composition and the preparation procedure. In recent years, the application of heterogeneous photocatalysis on the removal of contaminants in air and wastewater has fetched some interest [11–15]. Due to the high photocatalytic activity and stability of titanium dioxide, it is generally used as a photocatalyst for the removal of organic pollutants from water or air [16–20].

However, TiO_2 follows a relatively high electron–hole recombination rate, which is detrimental to its photoactivity. The doping of TiO_2 with transition metal ions like Ni(II) [21], Cu(II) [22], Nb(V) [23], Cr(III) [24,25], Fe(III) [26–29], and metal molybdates [13] were reported to improve the photocatalytic properties with enhanced absorption of visible/ultraviolet light. Binary metal oxides such as TiO_2/WO_3, TiO_2/MoO_3, TiO_2/SiO_2 and TiO_2/ZrO_2 have been widely studied for their unique chemical, physical and photocatalytic properties [30–33]. Studies with a $Fe_2O_3/SrTiO_3$ mixed oxide photocatalyst have shown improved photocatalytic activity for photo-oxidizing methanol under visible light irradiation [34]. Adel Ali Ismail has prepared the ternary heterogeneous mixed oxides i.e. $Y_2O_3/Fe_2O_3/TiO_2$ nanoparticles [35], which showed better photooxidation for EDTA than pure TiO_2. Recently, Fe_2O_3/TiO_2 heterogeneous mixed oxides [36–39] have shown better photocatalytic activity than pure TiO_2 for oxidation of different organic compounds such as methylene blue, chloroform and formaldehyde but it is inferior to Degussa P 25. In this study a homogeneous solution between Fe_2O_3 and TiO_2 has been made by high energy mechanical milling using various source of Fe^{3+} which shows high

* Corresponding author at: Department of Chemistry, West Bengal State University, Barasat, North 24 Pgs, Kolkata 700126, India. Tel.: +91 33 25241975; fax: +91 33 25241977.
E-mail address: tanmay_ghorai@yahoo.co.in (T.K. Ghorai).

0925-8388/$ – see front matter.
doi:10.1016/j.jallcom.2011.05.069

photochemical activity and it is more active than Degussa P 25 in visible light for oxidative degradation of various dyes. It is observed that the photocatalytic activity of Fe–Ti oxides alloy largely depends on iron content, preparative condition and sintering temperature having optical adsorption edge around 2.2 eV, which facilitates a strong absorption of visible light. The Fe_2O_3/TiO_2 alloys in different mole ratio were prepared by mechanical milling method (using a ball mill) and their photocatalytic activities were evaluated by the photooxidations of different dyes like Rhodamine B (RB), Methyl orange (MO), Thymol blue (TB) and Bromocresol green (BG) under visible light (300-W Xe lamp; $\lambda > 420$ nm) irradiation. The alloy of Fe_2O_3 (5 mol%) with TiO_2 (anatase) is a better photoactive material compared to Degussa P25 TiO_2 and other compositions of Fe_2O_3/TiO_2.

2. Experimental

2.1. Synthesis of Fe_2O_3/TiO_2 photocatalysts

A stoichiometric mixture of TiO_2 (Aldrich, 99.99%) and yellow/red Fe_2O_3 (5, 7 and 10 mol%) (99.9%, Tata-Pigment, India) was prepared by mechanical grinding in a planetary ball mill using small amount of water. This mechanical milling was allowed for 4 h for complete mixing of the oxides forming a solid solution. The milling was performed in Fritsch Pulverisette No. 6 planetary ball mill, using a rotational speed of 250 rpm at a constant rotation direction and a ball to powder weight ratio of 10:1. Both the container and balls were made of aluminium oxide. The prepared samples were dried at 100 °C for 15 h in an oven and photocatalytic activity was studied. The sources of Fe^{3+} were yellow iron oxide, red iron oxide and precipitated ferric hydroxide. The heat-treatment of the sample at a temperature higher than 200 °C had poor photocatalytic activity. Rhodamine B (RB), Methyl orange (MO), Thylmol blue (TB), Bromocresol green (BG) were A.R. reagents procured from MERCK India.

2.2. Photocatalytic experiment

Photocatalytic experiments were conducted using nanophotocatalysts in presence of photocatalytically degradable different dyes in water solution. The photocatalytic reaction was carried out under visible light irradiation with slow stirring (using magnetic stirrer) of the solution mixture and Fe_2O_3/TiO_2 photocatalysts. The light source was a 300-W Xe lamp (ILC technology; CERMAX LX-300F). The container was made of Petridis of volume 200 ml. The reactions were performed by adding nano powder of each photocatalyst (0.1 g) into each set of a 100 ml of different solution of dyes.

2.3. Analytical methods

A small volume (1 ml) of reactant liquid was siphoned out at regular interval of time for analysis. It was then centrifuged at 1100 rpm for 15 min, filtered through a 0.2 μm-millipore filter to remove the suspended catalyst particles and concentration of dye was measured by absorption spectrometry using UV-VIS spectrometer (UV-1601, SHIMADZU) at its wavelength of maximum absorption.

2.4. Characterization

The crystal structure of the prepared samples was determined by the X-ray diffractometer (XRD) (Model: Philips PW 1710) equipped with a Cu Kα radiation. The accelerating voltage and current used were 40 kV and 20 mA, respectively. The 2θ ranged from 15 to 70°.

Crystallite sizes (D) of the obtained powders were calculated by the X-ray line broadening technique performed on the direction of lattice using computer software (APD 1800, Philips Research Laboratories) based on Scherer's formula [40].

$$D = \frac{0.89\lambda}{\beta \cos\theta} \quad (1)$$

where D is the crystallite size, λ is the X-ray wavelength, θ is the Bragg's angle and β is half width. The stoichiometry of Fe_2O_3/TiO_2 alloys have been examined by energy dispersive X-ray spectroscopy (EDX) (JEOL JMS-5800) which is consistent with the amount taken of Fe_2O_3 and TiO_2 during synthesis.

The FT-IR analysis was performed using a Perkin-Elmer Paragon 1000 FT-IR spectrometer and BET surface area measurements were carried out using a BECKMAN COULTER SA3100 through nitrogen adsorption–desorption isotherm at 77 K. X-ray photoelectron spectroscopy (XPS) measurements were carried out in an Axis-Ultra X-ray photoelectron spectrophotometer in vacuum (1×10^{-5} Pa).

The UV–vis diffuse reflectance spectra of the prepared powders were obtained by a UV–VIS spectrophotometer (UV-1601 Shimadzu) at room temperature. The average sizes of nanoparticles were measured in the transmission electron microscopy (TEM) (Model Philips TM-30, Philips Research Laboratories).

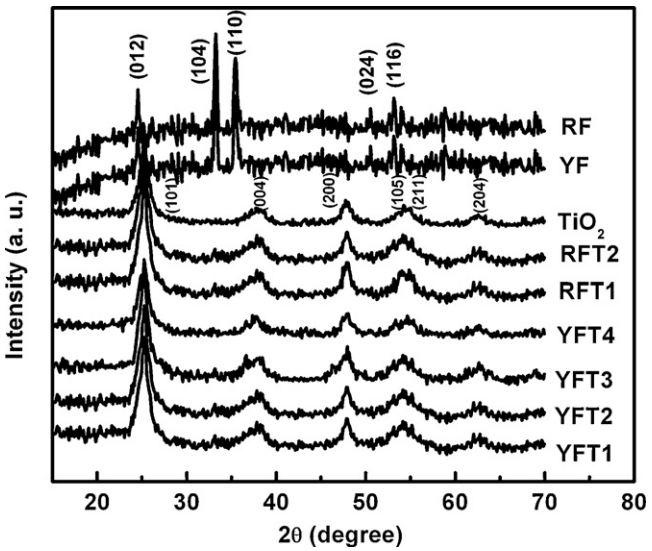

Fig. 1. A comparison of X-ray diffraction patterns of TiO_2, YFT1, YFT2, YFT3, YFT4, RFT1, RFT2, YF and RF nanopowders prepared by mechanochemical method after heat treatment at 100 °C for 15 h.

The magnetic susceptibility was measured by Guoy balance. The ESR spectrum was obtained by BRUCKER ER083CS model at room temperature (ca. 298 K).

3. Results and discussion

3.1. XRD analysis

Fig. 1 shows the XRD patterns of TiO_2, YFT1, YFT2, YFT3, YFT4, RFT1, RFT2, YF and RF (abbreviation presented in Table 1) mixed oxides nanopowders after heat treatment at 100 °C for 15 h in air atmosphere. It has been observed that the phases prepared at different molar ratios of mixed oxides TiO_2 and Fe_2O_3 (YFT1, YFT2, YFT4, RFT1 and RFT2) have anatase phase up to 5 mol% of Fe_2O_3 (as per JCPDS no. 84-1285), and YF, RF are hexagonal phases (as per JCPDS no. 86-0550). The XRD pattern of TiO_2 sample shows distinct peaks of the anatase phases, without any indication of rutile phases. XRD of YFT1, YFT2, YFT3, YFT4, RFT1 and RFT2 indicate no change of crystallographic characteristics before and after the photocatalytic reactions, which is shown in Fig. 1. XRD also indicate that the final products after ball milling have anatase phase of TiO_2 and Fe ions are well inserted into the framework of the TiO_2 anatase structure. The small incorporation of Fe^{3+} in TiO_2 will not change much of the XRD peaks. The change will be in first or second decimal of theta value, because ionic radius of Ti^{4+} and Fe^{3+} are very close (0.68 Å and 0.64 Å). Moreover magnetic data and EPR data does not infer any aggregation of Fe^{3+} as Fe_2O_3 crystal. Due to broad peaks of XRD we are unable to evaluate the accurate d – values of lattices. After photochemical reaction no metal ion leaching was observed. The sample prepared with red Fe_2O_3 and yellow Fe_2O_3 or precipitated $Fe(OH)_3$ gave same chemical and physical characteristics. Average crystallite sizes of the prepared photocatalysts were calculated according to Scherer's formula and indicated that the crystallite sizes of the samples were approximately (12–15 nm). The atomic level dispersion Fe_2O_3 in TiO_2 have been presented in Fig. 2 through energy dispersive X-ray spectroscopy,

3.2. Specific surface area (BET) analysis

The BET surface area of Fe_2O_3/TiO_2 composite powders (YFT1) calcined at 100 °C was 58.5 m^2/g, while the surface area of P25 is 49.1 m^2/g and the surface area of other prepared photocatalysts are presented in Table 1. Though surface area of YFT1, RFT1 and Degussa

Table 1
Resultant properties of YFT1, YFT2, YFT3, RFT1, RFT2, YFT4, FT, P25, YF and RF composites.

Sample	Acronym	S_{BET} (m^2/g)	Anatase crystal size (nm)	Absorption edge (nm)	Effective band gap energy (eV) (from optical spectra)
Yellow Fe_2O_3 (5 mol%)/TiO_2	YFT1	58.5	12.17	548	2.26
Yellow Fe_2O_3 (7 mol%)/TiO_2	YFT2	52.2	12.38	520	2.38
Yellow Fe_2O_3 (10 mol%)/TiO_2	YFT3	48.6	12.43	508	2.48
Red Fe_2O_3 (5 mol%)/TiO_2	RFT1	55.2	12.35	540	2.29
Red Fe_2O_3 (7 mol%)/TiO_2	RFT2	50.3	12.63	470	2.63
Yellow Fe_2O_3 (5 mol%)/TiO_2 (after reaction)	YFT4	58.5	12.22	548	2.26
$Fe(OH)_3$ (5 mol%)/TiO_2	FT	56.6	12.22	548	2.26
Degussa P25	P25	49.1	12.46	387	3.2
Yellow Fe_2O_3	YF	4.8	20.05	563	2.2
Red Fe_2O_3	RF	4.1	21.26	558	2.23

BET surface area measured by dinitrogen adsorption desorption isotherm at 77 K.

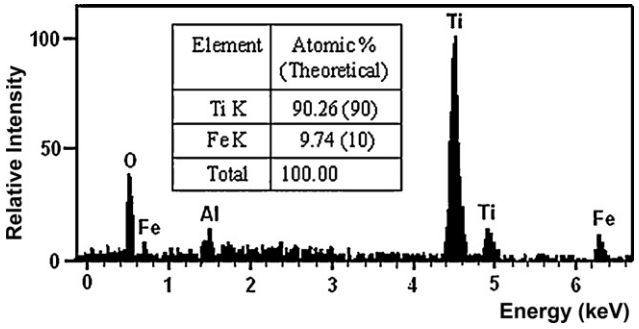

Fig. 2. EDX spectra of Fe_2O_3 (5 mol%)/TiO_2 (YFT1).

P25 are comparable, but photocatalytic activity of YFT1/RFT1 is merginally times greater than P25. Therefore, among all the prepared photocatalyst the YFT1/RFT1 is more photoactive for faster degradation of different dyes like RB, MO, TB and BG under visible light (300-W Xe lamp; $\lambda > 420$ nm).

3.3. Transmission electron microscopy (TEM) analysis

Nanoparticles with average size about 30 ± 5 nm were observed in the transmission electron microscopy (TEM) of YFT1. This has been shown in Fig. 3. The calculated crystallite size of YFT was about 12–13 nm obtained from XRD (shown in Table 1).

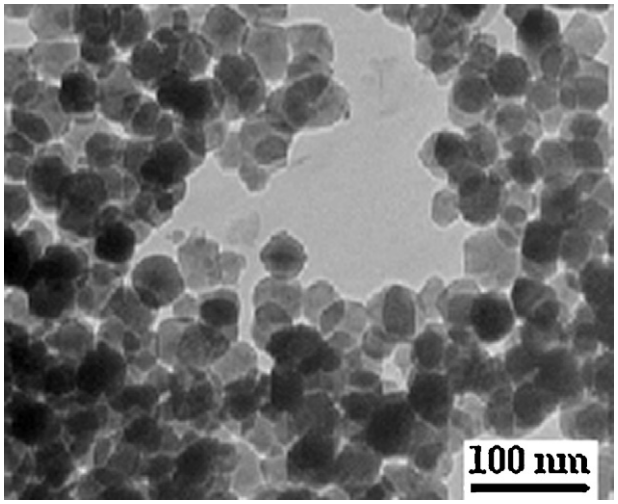

Fig. 3. TEM images of YFT1.

3.4. FT-IR spectra analysis

FT-IR spectra shown spectrum of YFT1, RFT1 and YFT4 are similar to TiO_2 shown in Fig. 4. This indirectly indicates that Fe_2O_3 has been dissolved into the TiO_2 lattices. The two bands observed at about 3400 and 1600 cm^{-1} are characteristic of the H–O bending mode of hydroxyl groups present on the surface due to moisture. These are crucial to the photocatalytic reactions since they can react with photoexcited holes generated on the catalyst surface and produce hydroxyl radicals [41], which act as powerful oxidant. The absorption band around 1200 cm^{-1} may be assigned to the Ti–O–Ti bending [37]. The absorption band at 609 cm^{-1} attributes to the Ti–O stretching vibrations of TiO_2 anatase phase and their small peaks around 1405 and 1050 cm^{-1} of samples YFT1, RFT1 and YFT4 were detected. There were no eminent peaks of undissolved Fe_2O_3. This indirectly indicates that Fe_2O_3 has been dissolved into the TiO_2 lattices and form solid solution. The new peaks (1405 and 1050 cm^{-1}) may be assigned to Ti–O–Fe hetero bond. In fact, a vibration frequency reduction would indicate a higher ionization of the metallic atom on which the molecule is adsorbed. The band at 1405 cm^{-1} is attributed to adsorbed dyes on Fe atoms and 1050 cm^{-1} attribute to carbonates. The presence of carbonate vibrations can be well resolved in all metastable alloy samples as shown in Fig. 4. The alloys on heating above 600 °C segregate into the pure phases of TiO_2 and Fe_2O_3. It shows that the alloys are metastable phases between TiO_2 and Fe_2O_3.

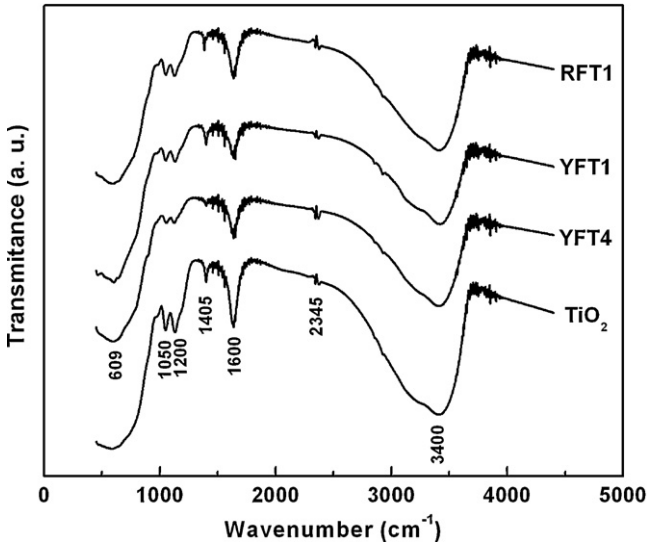

Fig. 4. FT-IR spectra for RFT1, YFT1, YFT4, and TiO_2 samples.

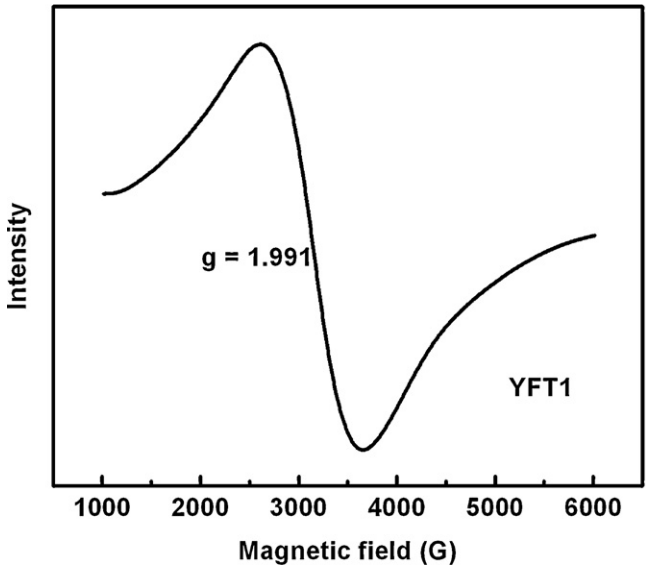

Fig. 5. EPR spectrum of YFT1.

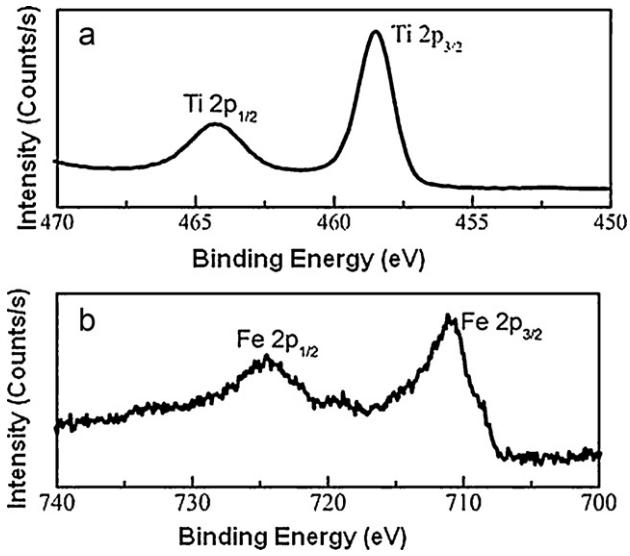

Fig. 7. XPS spectrum of YFT1 (a) Ti(2p) and (b) Fe(2p) core levels.

3.5. EPR spectrum study

Electronic paramagnetic resonance spectrum (EPR) of YFT1 shown in Fig. 5, reflected a signal at a g-tensor value of 1.991, indicating the presence of low spin state of Fe^{3+} in TiO_2 [42]. Due to absence of any hyperfine line in ESR spectra, it can be suggested that Fe^{3+} cations are well separated. No EPR signal was detected on pure TiO_2. The magnetic moment of YFT1/RFT1 is found to be 1.73 BM measured by Guoy's method. It indicates that the Fe^{3+} in YFT1/RFT1 alloy contains one unpaired electron. This infers that iron exists as a Fe^{3+} ion in the system under strong crystal field environment producing low spin Fe^{3+}. The magnetic moment does not change reasonably with lowering temperature which indicates that Fe–Fe spin interaction is absent (shown in Fig. 6) at 5 mol% of Fe_2O_3.

3.6. Oxidation states of Fe ion (XPS study)

The oxidation states of Fe^{3+} have been determined by redox titration and XPS. Known amount of catalyst is treated with HF and KBr in absence of air (under argon atmosphere and was back titrated with Mohr salt solution (Fe^{2+})). No Fe^{2+} of Mohr salt solution was consumed in the titration. This indicates the absence of any higher oxidation states (4+/5+/6+) of Fe. Any higher oxidation of Fe could liberate Br_2 and would have been consumed by Fe^{2+}. Fig. 7a shows the XPS analysis of Fe_2O_3/TiO_2 covering the Ti photoemission peaks. The binding energy of Ti 2p1/2 was observed to be at approximately 464.5 eV, which corresponds well with the handbook data for Ti^{4+}. However, the binding energy of Ti 2p3/2 was 458.9 eV, which is slightly lower than the handbook data. The splitting data between the Ti 2p1/2 and Ti 2p3/2 core levels is 5.6 eV indicating a normal state of Ti^{4+} in the anatase TiO_2. Fig. 7b shows the XPS spectra covering the Fe(2p) peaks. The Fe(2p) core level are split into Fe2p1/2 and Fe2p3/2 due to spin orbit coupling and appear at their normal positions that is 724.7 eV and 710.8 eV respectively. The XPS spectra do not show any elemental Fe peak. A hump at ~719 eV is characteristic of presence of Fe^{3+}. However, this result may be due to formation of only Ti^{4+} and Fe^{3+} chemical states in the samples (as can be seen from the Ti(2p) and Fe(2p) core levels XPS). The XPS data are in line with earlier observations and strongly support the formation of TiO_2/Fe_2O_3 alloy [43–46]. The surface atomic concentration of the Fe_2O_3 (5 mol%)/TiO_2 alloy estimated from XPS are shown in Table 2. The surface atom concentrations for oxygen, titanium and iron atoms and the atomic ratio for Fe/Ti (10.24) were obtained from the results of XPS analysis. The atomic ratio data were in conformity with the EDAX data.

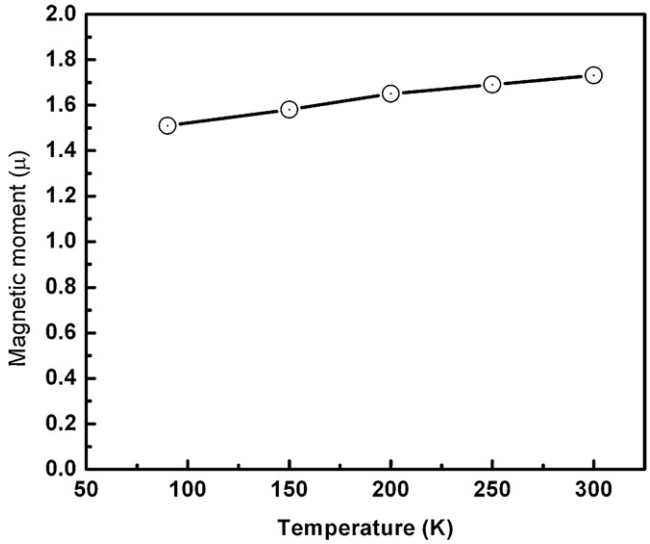

Fig. 6. Magnetic susceptibility measurement of YFT1.

3.7. Photocatalytic activity of the prepared samples

The photooxidation of different coloured dyes solution like RB, MO, TB and BG to colourless solution under prepared photocatalysts and visible light (300-W Xe lamp; $\lambda > 420$ nm) irradiation is shown in Figs. 8–11 respectively. UV–vis spectra of RB, MO, TB and BG taken after the irradiation with Fe_2O_3/TiO_2 compositions (YFT1, YFT2, YFT3, RFT1, RFT2, P25, YF and RF) were measured and corresponding absorbance of dyes were found at 554, 464, 597 and 616 nm respectively. The different dyes were found to be completely decolorized after the irradiation. It required about 60 min for RB, 90 min for MO, 105 min for TB, and 150 min for BG for complete decolorization. Comparatively the rate of degradation of Rhodamine B is faster among all the four dyes. For all the cases the catalysts were taken at 1 g/l and different dye concentration was about 10 mM. The photocatalytic activities have presented

Table 2
The surface atom concentration for oxygen, Fe and Ti atoms of the Fe_2O_3 (5 mol%)/TiO_2 alloys by XPS.

Sample	Atomic surface concentration (%)			Surface atomic ratio (%)
	O	Ti	Fe	Fe/Ti
Fe_2O_3 (5 mol%)/TiO_2	67.29	29.67	3.04	10.24

Table 3
Degradation rate constants of different organic dyes in different pH using different photocatalysts of YFT1, YFT2, YFT3, RFT1, FRT2, FT, P25, YF and RF.

Dyes	pH	Reaction rate constant k ($\times 10^{-3}$ min^{-1})								
		YFT1	YFT2	YFT3	RFT1	RFT2	FT	P25	YF	RF
RB	7.01	84.30	61.40	50.10	62.67	49.51	70.65	15.09	1.33	0.89
MO	6.99	39.44	31.28	20.63	34.38	20.24	33.83	11.75	0.98	0.58
TB	8.01	37.12	23.20	14.29	27.80	15.85	26.36	10.74	0.38	0.23
BG	8.03	13.87	10.51	5.10	12.13	6.70	12.81	7.86	0.54	0.26

RB, Rhodamine B; MO, Methyl orange; TB, Thymol blue; BG, Bromocresol green.
The concentration of the different dyes is ~10 mM.
The catalyst concentration is $C_{catalysts}$ = 1 g/l. Time required for 50% decolorization of different organic dyes solution. All photocatalysts are calcined at 100 °C for 15 h.

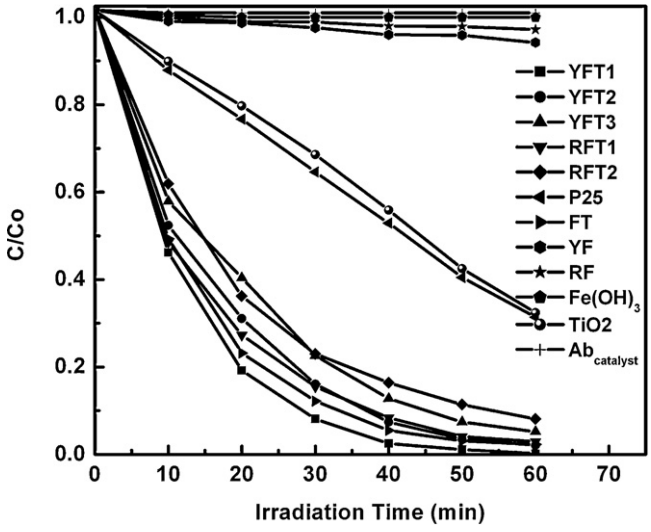

Fig. 8. The Rhodamine B oxidation in UV–vis absorption spectra at 554 nm as a function of visible light irradiation time in the prepared photocatalysts calcined at 100 °C for 15 h, and absence of catalyst ($Ab_{catalyst}$), 300-W Xe lamp with a cutoff filter ($\lambda > 420$ nm).

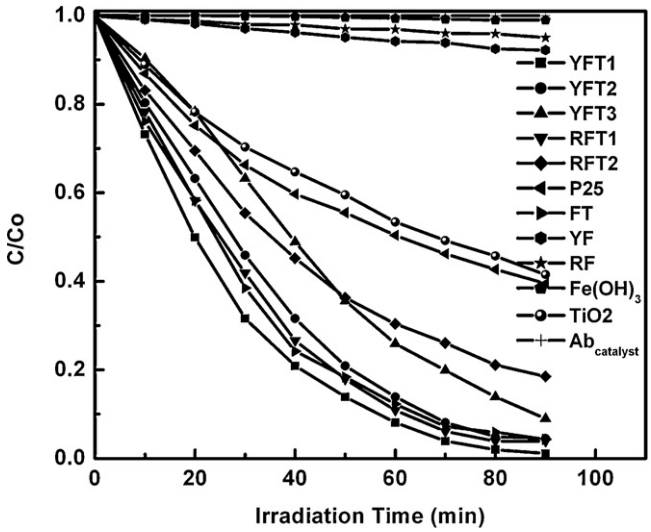

Fig. 9. The Methyl orange oxidation in UV–vis absorption spectra at 464 nm as a function of visible light irradiation time in the prepared photocatalysts calcined at 100 °C for 15 h, and absence of catalyst ($Ab_{catalyst}$), 300-W Xe lamp with a cutoff filter ($\lambda > 420$ nm).

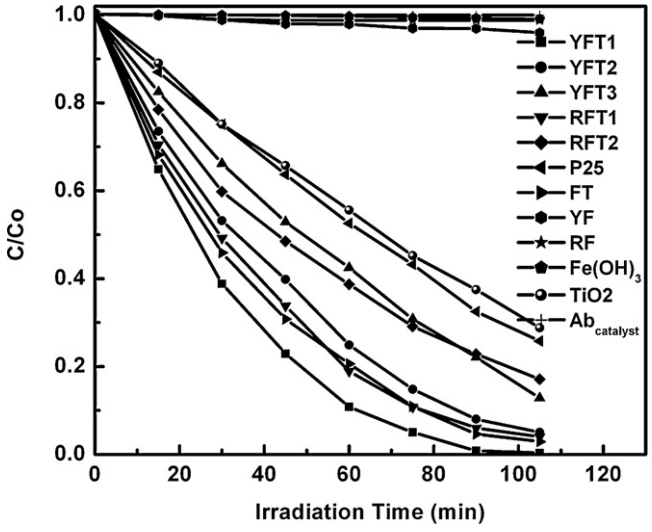

Fig. 10. The Thymol blue oxidation in UV–vis absorption spectra at 597 nm as a function of visible light irradiation time in the prepared photocatalysts calcined at 100 °C for 15 h, and absence of catalyst ($Ab_{catalyst}$), 300-W Xe lamp with a cutoff filter ($\lambda > 420$ nm).

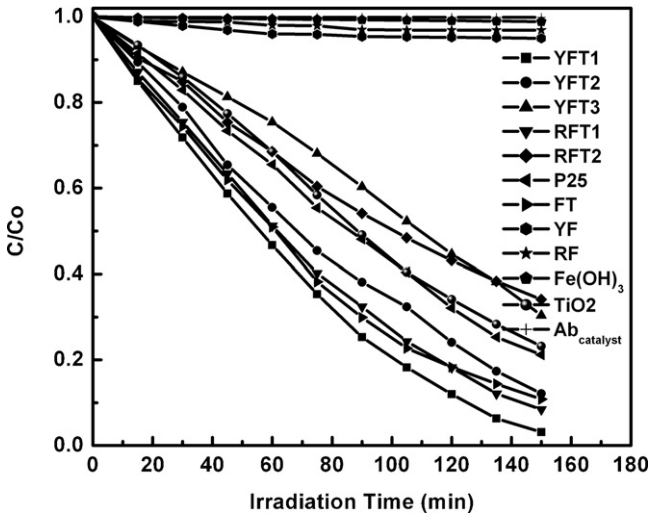

Fig. 11. The Bromocresol green oxidation in UV–vis absorption spectra at 616 nm as a function of visible light irradiation time in the prepared photocatalysts calcined at 100 °C for 15 h, and absence of catalyst ($Ab_{catalyst}$), 300-W Xe lamp with a cutoff filter ($\lambda > 420$ nm).

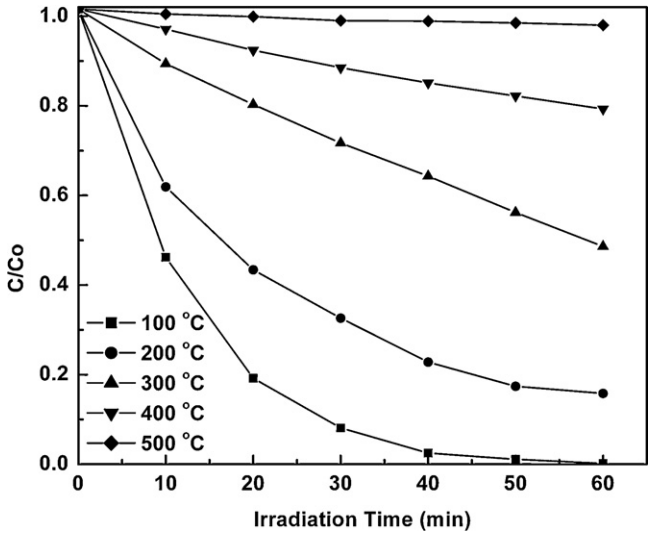

Fig. 12. The effect of calcinations temperature for 15 h for 100 °C, 200 °C and other temperature is for 2 h on the photocatalytic activity of YFT1, the catalyst concentration is $C_{catalysts}$ = 1 g/l. Rhodamine B concentration is C_{RB} = 10 mM, 300-W Xe lamp with a cutoff filter (λ > 420 nm).

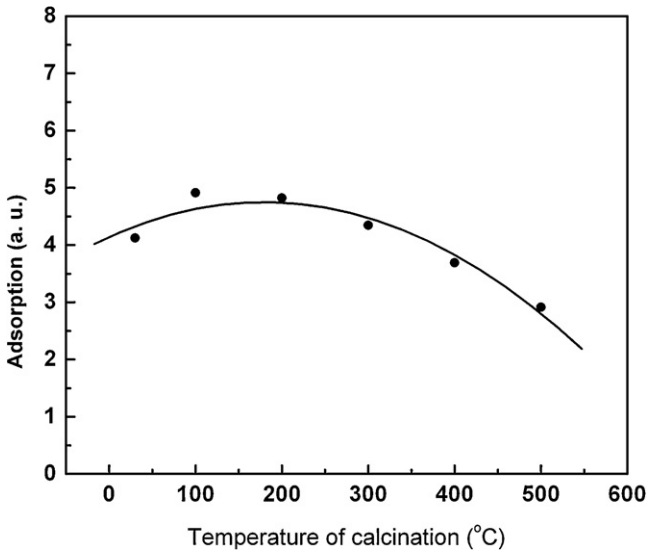

Fig. 13. Adsorption of dyes on photocatalysts calcined at different temperature.

in Figs. 8–11. Under visible light irradiation, the alloy YFT1/RFT1 powder exhibited highest photocatalytic activity than that of other compositions of Fe_2O_3/TiO_2 mixed oxides, P25 TiO_2, and pure yellow/red Fe_2O_3 for all the four dyes solutions. It is also observed that in absence of catalyst the degradation of dyes is not possible under visible light (shown in Figs. 8–11). The YFT1/RFT1 alloy powders have shown five times higher photocatalytic activity than that of P25 in case of Rhodamine B and three times higher photoactivity than that of P25 in case of other three dyes (MO, TB and BG). The increment of Fe_2O_3 concentration beyond 5 mol% leaded lower photocatalytic activity. The degradation rate constant (k) for RB, MO, TB and BG using YFT1, YFT2, YFT3, RFT1, RFT2, P25, YF and RF photocatalysts have been presented as the time required for 50% decolourization of dyes solutions in Table 3. The photocatalytic activity is independent of source of Fe^{3+} like yellow oxide or red-oxide or precipitated ferric hydroxide.

3.8. Effect of heat-treatment for photocatalyst on the photocatalytic activity

The effect of heat-treating temperature of alloys on the photocatalytic activity was also investigated. Fig. 12 shows the profiles of the photooxidations of Rhodamine B to CO_2 under visible light (λ > 420 nm) irradiation using YFT1 alloy calcined at 100 °C, 200 °C, 300 °C, 400 °C and 500 °C. The samples calcined at 100 °C showed highest photocatalytic activity than that calcined at other temperatures. It seems that the increase of the calcination temperature decreases the defect-states on the surface. Above 100 °C the activity of catalyst decreases with rise of calcination temperatures and decrease of specific surface area. This may be due to the change of the particle size and surface area. The IR spectrum does not show presence of any absorbed lattice water. It is also observed that adsorption of dye (RB, MO, TB, and BG) decreases with increase of heat treatment temperature of the catalyst. This is probably due to decrease of defect-structure on the surface of solid catalyst. Thus defect structure signifies its crucial role for photocatalytic activity. The effect of calcination temperature on the adsorption of dyes by photocatalysts is presented in Fig. 13. It indicates that adsorption of photocatalysts is maximum when calcinations temperature is 100 °C.

3.9. UV–vis diffuse reflectance spectrum

The UV–vis diffuse reflectance spectrum of alloys of Fe_2O_3/TiO_2 and pure TiO_2 have been presented in Fig. 14. It has reflected distinct absorption edges at 548 nm, 540 nm, nm, 520 nm, 508 nm, 470 nm, 563 nm, 558 nm and 387 nm for YFT1, RFT1, YFT2, YFT3, RFT2, YF, RF and pure TiO_2 respectively and corresponding band edge energies are 2.26, 2.29, 2.38, 2.44, 2.63, 2.2, 2.22 and 3.20 eV respectively as presented in Table 1. With increase of Fe^{3+}, the band end edge position shifted to slightly higher energy value possibly due to more inclusion of defect structures. With increasing the dopant concentration, the band edge energy increases, as a consequence the photocatalytic activity decreases. This may be assigned to the absorption edge increases to higher wave length, then it cover more frequency and transition probability at higher frequency will be more (it easily understood from the spectra). This causes the increase of efficiency. YFT1 photocatalysts has lower band gap energy (2.26 eV) with highest photocatalytic activity compared to other Fe_2O_3/TiO_2 alloys and P25. Further decrease of concentration of Fe^{3+} may decrease the band edge but it may reduce kinetics of reaction resulting in lower photo-catalytic activity.

3.10. Tentative mechanism of photosensitization of Fe_2O_3/TiO_2 (YFT/RFT) under visible light irradiation

The tentative mechanism of photooxidation may be as follow. As the band edge of Fe^{3+} is lower than TiO_2, which means that Fe^{3+} is situated in between conduction band (CB) and valence band (VB). The optical absorption leads to the formation of hole on Fe^{3+} and the liberated electron goes to conduction band. This charge separation is facilitated by visible light rather than UV or near UV light due to lesser energy gap between Fe^{3+} and bottom of conduction band. The role of the TiO_2 in the second photocatalytic process in Fig. 15 is in presence of visible light, Fe(III) in TiO_2 matrix generates Fe^{2+}, Fe^{4+} and charge-pair (e^-/h^+) and at the same time Fe^{3+} is also regenerated through electron or hole trapping by reversible reaction [44–48]. The exited electron is trapped in CB through the formation of super oxide radical anion $O_2^{\bullet -}$ using O_2 from the atmosphere on the surface and $e^-(Fe^{2+})$. On the other side the dye is sensitized and the dye cation is formed with the help of irradiation of visible light of λ > 420 nm and $e^-(Fe^{2+})$. The dye cation is unstable and decomposes injecting an electron in the conduction band of Fe^{2+}. The Fe^{2+} initiates the oxidative degradation of organic

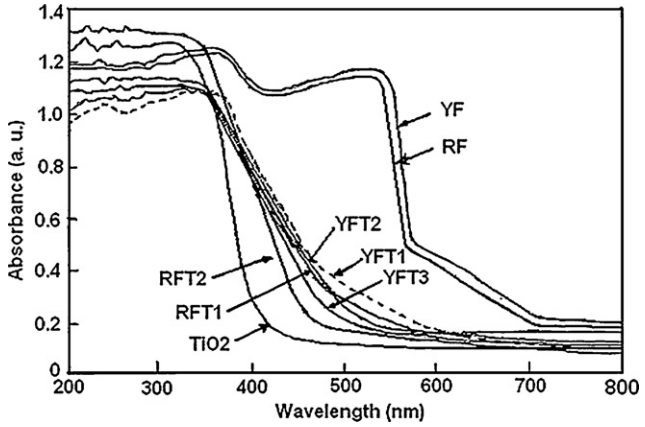

Fig. 14. UV–vis diffuse reflectance spectra of synthesized YFT1, YFT2, YFT3, RFT1, RFT2, RFT3, TiO_2, YF and RF powders.

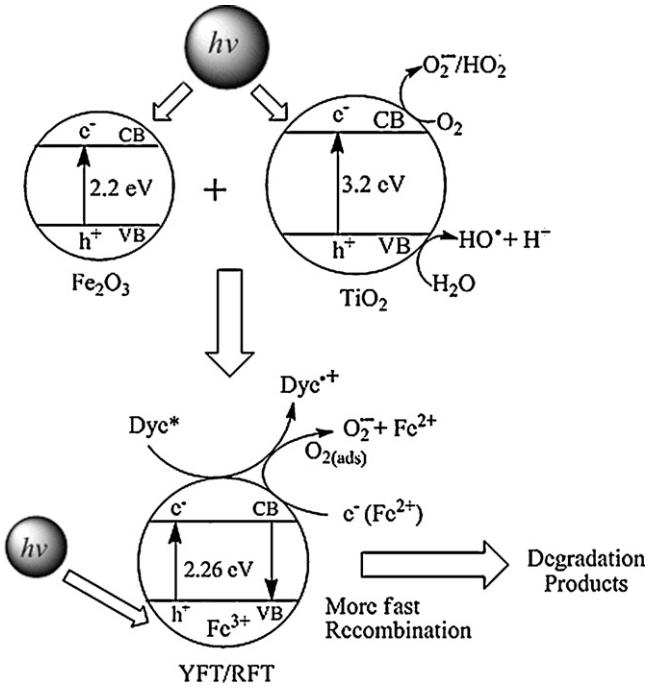

Fig. 15. Tentative schematic diagram of reaction mechanism of YFT/RFT photocatalysts under visible light irradiation.

compounds further assisted by super oxide radical. The schematic diagram of reaction mechanism is presented in Fig. 15.

4. Conclusions

Synthesis of nano-sized homogeneous solid solution between Fe_2O_3 and TiO_2 with high photocatalytic activity for oxidative degradation of different dyes was successfully obtained through mechanochemical synthesis. XRD data shows the formation of solid solution having anatase structure with no free Fe_2O_3 up to 5 mol% of Fe_2O_3. The chemical and physical natures of the materials remain same irrespective of source of Fe_2O_3. Fe_2O_3/TiO_2 catalyst have crystallite size about 12–13 nm measured from XRD and particle size about 30 ± 5 nm measured from TEM. FT-IR of all Fe_2O_3/TiO_2 prepared catalysts is similar to pure TiO_2. This indicates that Fe_2O_3 is dissolved into the TiO_2 lattices. The maximum solubility of Fe_2O_3 in TiO_2 is 5 mol% of Fe_2O_3 irrespective of source and this composition has highest photocatalytic activity that is 3–5 times higher than P25 TiO_2 for the oxidation of different dyes. We also observed that the rate of degradation of Rhodamine B is faster among all the four dyes under prepared catalyst and visible light.

Acknowledgements

This work was supported by the Council of Scientific and Industrial Research, India. The authors are grateful for its financial support.

References

[1] Y. Yang, X-jun Li, J-tao Chen, L-yan Wang, J. Photochem. Photobiol. A: Chem. 163 (2004) 517–522.
[2] M.R. Hoffmann, S.T. Martin, W. Choi, D.W. Bahnemann, Chem. Rev. 95 (1995) 69.
[3] L.A. Linsebigler, G. Lu Jr., J.T. Yates, Chem. Rev. 95 (1995) 735.
[4] M. Janus, A.W. Morawski, Appl. Catal. B: Environ. 75 (2007) 118–123.
[5] V. Stengl, S. Bakardjieva, N. Murafa, J. Subrt, H. Mestankova, J. Jirkovsky, Mater. Chem. Phys. 105 (2007) 38–46.
[6] A. Fujishima, K. Honda, Nature 238 (1972) 37–38.
[7] W. Wang, J. Zhang, F. Chen, D. He, M. Anpo, J. Colloid Interface Sci. 323 (2008) 182–186.
[8] P. Vijayan, C. Mahendiran, C. Suresh, K. Shanthi, Catal. Today (2008), doi:10.1016/j.cattod.2008.04.
[9] Z. Ambrus, N. Balazs, T. Alapi, G. Wittmann, P. Sipos, A. Dombi, K. Mogyorosi, Appl. Catal. B: Environ. 81 (2008) 27–37.
[10] J. Zhu, J. Ren, Y. Huo, Z. Bian, H. Li, J. Phys. Chem. C 111 (2007) 18965–18969.
[11] D. Beydoun, H. Tse, R. Amal, G. Low, S. McEvoy, J. Mol. Catal. A: Chem. 177 (2002) 265–272.
[12] T. Ohno, K. Sarukawa, M. Matsumura, J. Phys. Chem. B 105 (2001) 2417–2420.
[13] T.K. Ghorai, D. Dhak, S.K. Biswas, S. Dalai, P. Pramanik, J. Mol. Catal. A: Chem. 273 (2007) 224–229.
[14] J-Chuan Xu, Y-Li Shi, J-Er Huang, B. Wang, H-Lin Li, J. Mol. Catal. A: Chem. 219 (2004) 351–355.
[15] M.A. Hasnat, M.M. Uddin, A.J.F. Samed, S.S. Alam, S. Hossain, J. Hazard. Mater. 147 (2007) 471–477.
[16] A. Fuerte, M.D. Hernandez-Alonso, A.J. Maira, A. Martinez-Arias, M. Fernandez-Garcia, J.C. Conesa, J. Soria, Chem. Commun. (2001) 2718–2719.
[17] I.K. Konstantinou, T.A. Albanis, Appl. Catal. B: Environ. 49 (2004) 1–14.
[18] Y. Chen, K. Wang, L. Lou, J. Photochem. Photobiol. A: Chem. 163 (2004) 281–287.
[19] C.H. Kwon, H. Shin, J.H. Kim, W.S. Choi, K.H. Yoon, Mater. Chem. Phys. 86 (2004) 78–82.
[20] J.C. Colmenares, M.A. Aramendia, A. Marinas, J.M. Marinas, F.J. Urbano, Appl. Catal. A: Gen. 306 (2006) 120–127.
[21] D. Jing, Y. Zhang, L. Guo, Chem. Phys. Lett. 415 (2005) 74–78.
[22] G. Colon, M. Maicu, M.C. Hidalgo, J.A. Navio, Appl. Catal. B: Environ. 67 (2006) 41–51.
[23] K. Tennakone, J. Bandara, Sol. Energy Mater. Sol. Cells 60 (2000) 361.
[24] N. Serpone, D. Lawless, Langmuir 10 (1994) 643.
[25] J.C. Yu, G. Li, X. Wang, X. Hu, C.W. Leung, Z. Zhang, Chem. Commun. (2006) 2717–2719.
[26] J. Zhu, W. Zheng, B. He, J. Zhang, M. Anpo, J. Mol. Catal. A: Chem. 216 (2004) 35–43.
[27] Z. Zhang, C. Wang, R. Zakria, J.Y. Ying, J. Phys. Chem. B 102 (1998) 10871–10878.
[28] M.I. Litter, J.A. Navio, J. Photochem. Photobiol. A: Chem. 98 (1996) 171–181.
[29] J. Feng, R.S.K. Wong, X. Hu, P.L. Yue, Catal. Today 98 (2004) 441–446.
[30] Y.R. Do, W. Lee, K. Dwight, A. Wold, J. Solid State Chem. 108 (1994) 198.
[31] J. Papp, S. Soled, K. Dwight, A. Wold, Chem. Mater. 6 (1994) 496.
[32] X. Fu, L.A. Clark, Q. Yang, M.A. Anderson, Environ. Sci. Technol. 30 (1996) 647.
[33] Z. Liu, J. Davis, J. Phys. Chem. 98 (1994) 1253.
[34] H. Zhang, X. Wu, Y. Wang, X. Chen, Z. Li, T. Yu, J. Ye, Z. Zou, J. Phys. Chem. Solids 68 (2007) 280–283.
[35] A.A. Ismail, Appl. Catal. B: Environ. 58 (2005) 115–121.
[36] E. Celik, A.Y. Yildiz, N.F. Ak Azem, M. Tanoglu, M. Toparli, O.F. Emrullahoglu, I. Ozdemir, Mater. Sci. Eng. B 129 (2006) 193–199.
[37] M. Kang, Suk-Jin Choung, J.Y. Park, Catal. Today 87 (2003) 87–97.
[38] J. Yang, D. Li, Z. Zhang, Q. Li, H. Wang, J. Photochem. Photobiol. A: Chem. 137 (2000) 197–202.
[39] L. Diamandescu, M. Feder, D. Tarabasanu-Mihaila, F. Vasiliu, Appl. Catal. A: Gen. 325 (2007) 270–275.
[40] P. Klug, L.E. Alexander, Direction Procedures for Polycrystalline and Amorphous Materials, Wiley, New York, 1954.
[41] Z. Ding, G.Q. Lu, P.F. Greenfield, J. Phys. Chem. B 104 (2000) 4815.
[42] C. Adan, A. Bahamonde, M. Fernandez-Garcia, A. Martinez-Arias, Appl. Catal. B: Environ. 172 (2007) 11–17.
[43] Z. Yuan, J. Zhang, B. Li, J. Li, Thin Solid Films 515 (2007) 7091–7095.
[44] X. Zhang, L. Lei, Appl. Surf. Sci. 254 (2008) 2406–2412.
[45] O. Akhavan, R. Azimirad, Appl. Catal. A: Gen. 369 (2009) 77–82.
[46] O. Akhavan, Appl. Surf. Sci. 257 (2010) 1724–1728.
[47] Wen-Chi Hung, Ssu-Han Fu, Jeou-Jen Tseng, Hsin Chu, Tzu-Hsing Ko, Chemosphere 66 (2007) 2142–2151.
[48] T.K. Ghorai, S.K. Biswas, P. Pramanik, Appl. Surf. Sci. 254 (2008) 7498–7504.